Ordered Nanoparticles

DOI: 10.1002/anie.200700087

Ordered Three-Dimensional Arrays of Monodispersed Mn_3O_4 Nanoparticles with a Core–Shell Structure and Spin-Glass Behavior**

*Feng Jiao, Andrew Harrison, and Peter G. Bruce**

Nanoparticulate transition-metal oxides can exhibit enhanced optical, magnetic, and electrical properties when compared with their bulk counterparts, rendering such nanoparticles of interest for a variety of applications, for example, as electrodes in energy storage devices, as catalysts, and as magnetic storage devices.[1,2] Such size-dependent properties make the synthesis of monodispersed particles of great importance.[3–6] The properties of nanoparticles may also be influenced by the formation of core–shell structures or by assembling the particles into regular arrays.[6] However, the synthesis of nanoparticles that are monodispersed, exhibit a core–shell structure, or form ordered arrays, can be difficult. Herein we report, for the first time, the synthesis of monodispersed Mn_3O_4 nanoparticles, each encased in a shell of MnO_2, which spontaneously self-assemble into three-dimensional ordered arrays with cubic symmetry. The arrays exhibit spin-glass behavior rather than the superparamagnetism anticipated for nanoparticles.

The higher surface-area-to-volume ratio of nanoparticles compared with particles of micron dimensions makes the presence of a core–shell structure of much greater significance for the physical properties of nanomaterials compared with their bulk counterparts. However, the techniques that are invariably used to characterize nanomaterials (transmission electron microscopy (TEM), powder X-ray diffraction (PXRD), and N_2 adsorption) are not well-suited to identify a shell, especially if it is thin or amorphous. Characterizing core–shell structures presents a greater challenge, because it necessitates the use of a combination of bulk and surface methods. While the deliberate synthesis of core–shell structured nanoparticles is often difficult, the dominance of TEM and PXRD as characterization tools for nanomaterials may have resulted in core–shell structures going undetected. Indeed, a reexamination of nanoparticulate materials, especially of those whose physical properties may have proved difficult to interpret under the assumption of homogeneous nanoparticles, is to be recommended.

Manganese oxides are particularly important, because they find use in many applications.[7] Synthesis of core–shell Mn_3O_4–MnO_2 particle arrays was carried out by modifying a method used previously to form MnO_x nanoparticles.[3] There were no previous reports of Mn_3O_4–MnO_2 core–shell nanoparticles or three-dimensional ordered Mn_3O_4 arrays synthesized by this or any other method. Nanoparticles, prepared as described in the Experimental Section, were examined by TEM (Figure 1). The monodispersity of the particle size is evident in Figure 1a and is repeated throughout the entire sample. The particles have an average size of 7.8 ± 0.5 nm, on

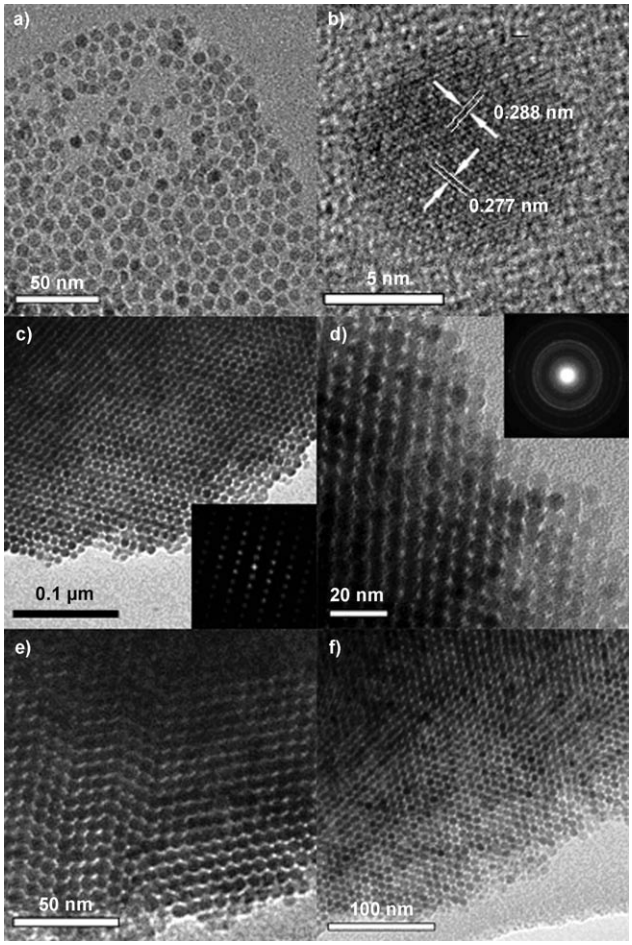

Figure 1. a) TEM image of isolated Mn_3O_4 nanoparticles; b) HRTEM image of a single Mn_3O_4 nanoparticle; c)–f) TEM images of different regions of highly ordered Mn_3O_4 nanoparticle arrays. Fourier transform image of (c) is shown in the inset. The SAED pattern is shown in the inset of (d).

[*] F. Jiao, Prof. P. G. Bruce
EaStChem, School of Chemistry
University of St. Andrews
The Purdie Building, North Haugh, St Andrews KY16 9ST (UK)
Fax: (+44) 1334-463-808
E-mail: p.g.bruce@st-and.ac.uk
Prof. A. Harrison[+]
EaStChem, School of Chemistry
University of Edinburgh
Joseph Black Building, West Mains Road, Edinburgh EH9 3JJ (UK)
[+] Current address:
Institut Laue-Langevin
6, rue Jules Horowitz, BP 156, 38042 Grenoble Cedex 9, (France)

[**] PGB is grateful to the Royal Society, EU, and the EPSRC for financial support.

the basis of TEM analysis. High-resolution TEM (HRTEM) studies of individual particles (Figure 1b) revealed their single-crystal nature, and the lattice spacings marked on the Figure correspond well with the [200] and [103] d spacings, 0.288 nm and 0.277 nm, respectively, obtained for Mn_3O_4 from the JCPDS database (JCPDS No. 24-734). Selected-area electron diffraction (SAED) (Figure 1d, inset) shows clear diffraction rings, which can be indexed on the Mn_3O_4 spinel structure, in agreement with the HRTEM results. Although no surface layer or coating on the Mn_3O_4 nanoparticles could be unambiguously observed by HRTEM analysis, evidence that the Mn_3O_4 nanoparticles are coated with a thin MnO_2 layer, that is, that the particles have a core–shell structure, is discussed below.

The formation of monodispersed nanoparticles depends on controlling nucleation and growth. Monodispersity can be induced by ensuring homogeneous nucleation with subsequent diffusion-controlled growth.[8] Heating $[Mn(acac)_2]$ (acac = acetylacetonate) in air at 210 °C in the absence of oleylamine resulted in large Mn_3O_4 particles distributed over a range of particle sizes, thus confirming that the alkyl amine plays a critical role in forming monodispersed nanoparticles. Heating $[Mn(acac)_2]$ to its decomposition temperature while stirring it vigorously in oleylamine ensured multiple nucleation. Diffusion of growth species through the highly viscous oleylamine solution to the many growing crystallites will be slow, thus limiting crystallite growth. These conditions are favorable for the growth of monodispersed particles, as observed.

Efforts were made to vary the size of nanoparticles and the ratio of core to shell; parameters such as heating time and temperature, composition of the $[Mn(acac)_2]$/oleylamine mixture, and length of alkyl chain on the surfactant were all explored, but their variation invariably resulted in either no reaction, a loss of monodispersity, or formation of bulk Mn_3O_4. Carrying out the synthesis in air rather than in an inert atmosphere is key to the formation of the core–shell structure, with atmospheric O_2 oxidizing the Mn_3O_4 surface to MnO_2. However, varying the temperature and time did not alter the degree of MnO_2 shell formation.

Examination of the Mn_3O_4 material without dispersion in hexane revealed that the Mn_3O_4 particles had spontaneously self-assembled into highly ordered three-dimensional close-packed arrays, Figures 1c–f and inset of Figure 1c. Studying the arrays from different directions established that the predominant symmetry adopted by close packing the approximately spherical particles was cubic, although there is clear evidence of stacking faults and even some minor regions that exhibit hexagonal packing (Figure 1e,f). Although energetics clearly dictate that the spherical particles adopt a close-packed arrangement, there is no evidence for alignment of the crystallographic directions between different particles, as is evident from the selected-area electron diffraction experiment (inset Figure 1d), which exhibits powder-diffraction-like rings, not single-crystal behavior. Examination of many regions of the material demonstrated that the 3D ordered arrays exist throughout.

Confirmation that the material is Mn_3O_4, with the normal spinel structure, was obtained by powder X-ray diffraction (Figure 2). Excellent agreement between the diffraction pattern for the nanocrystalline arrays and bulk Mn_3O_4 is evident. The peaks associated with the former pattern are of course broader owing to the smaller particle size. Application

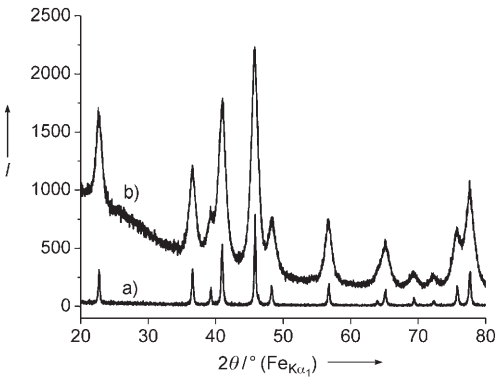

Figure 2. PXRD patterns for a) bulk Mn_3O_4 and b) Mn_3O_4 nanoparticle arrays.

of the Debye–Sherrer formula relating peak width to particle size gave a particle size of 8.1 nm, in good agreement with the value obtained from TEM data (7.8 nm). Note that the Debye–Sherrer formula assumes isotropic particles, which is accurate in the case of the cubic spinel.

The ease with which the arrays could be dispersed in nonpolar solvents, such as hexane, suggested that the surface of the particles was capped by the alkyl amine surfactant, thus presenting a hydrophobic exterior. To investigate this effect, FTIR spectra were collected for the array, as shown in Figure 3 (which also includes the spectrum of oleylamine for

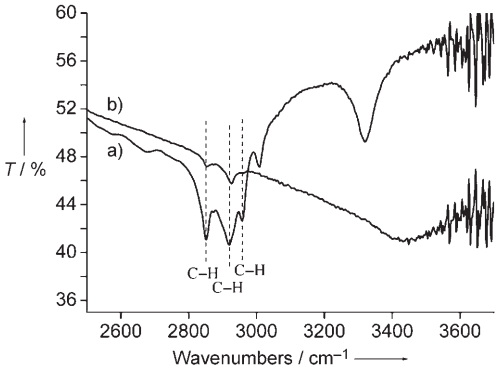

Figure 3. FTIR spectra for a) oleylamine and b) Mn_3O_4 nanoparticle array. T = transmission.

comparison). Examination of these results revealed that the major peaks of oleylamine are also present in the spectrum collected from the array, consistent with the presence of the alkyl amine on the surface of the particles. Whereas the C–H vibrations of the oleylamine and the array match very well, there is a shift in the NH_2 vibrations from 3319 cm^{-1} for the oleylamine to 3446 cm^{-1} for the Mn_3O_4 array.[9,10] Such a shift is consistent with coordination of Mn centers by the NH_2

group of the alkyl amine, and similar shifts have been noted for other alkyl amine based ligands coordinating to transition-metal ions.[10] Further confirmation for the presence of the alkyl amine in the array was obtained by elemental analysis, which yielded an N content of 0.56 wt %.

The DC magnetization measurements on the Mn_3O_4 array (Figure 4) revealed some form of magnetic transition a little

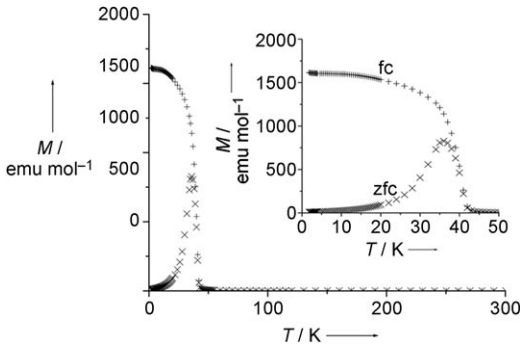

Figure 4. DC magnetization of Mn_3O_4 nanoparticles measured after cooling in zero field (zfc, ×) then in a field of 0.01 T (fc, +). The inset reveals the responses near the fc–zfc splitting in greater detail.

above 40 K: there is a splitting of the field cooled (fc) and zero field cooled (zfc) response below about 44(1) K, and the zfc data show a maximum at 36.0 K. Bulk Mn_3O_4 is known to order magnetically at $T_c = 42$ K to produce a collinear ferrimagnetic array. On further cooling, a spiral spin structure and subsequently a canted spin array is formed.[11] Nanoparticulate forms of the material also show a spontaneous moment below a blocking temperature, T_B, somewhat lower than 42 K.[3,12] Values of 36, 40, and 41 K have been reported for T_B for particle sizes of 6, 10, and 15 nm, respectively.[3]

Given that the present work represents the first report of a 3D array of Mn_3O_4 nanoparticles, it is interesting to investigate whether there is any evidence that the nanoparticles are magnetically isolated (in which case superparamagnetism is anticipated), or if there is magnetic interaction between them (especially if the surface coverage by the alkyl amine was incomplete). The AC susceptibility provides further insight. Figure 5 shows the change in the real part of the AC susceptibility with probe frequency (ν) and temperature, revealing an increase in T_B as ν increases.

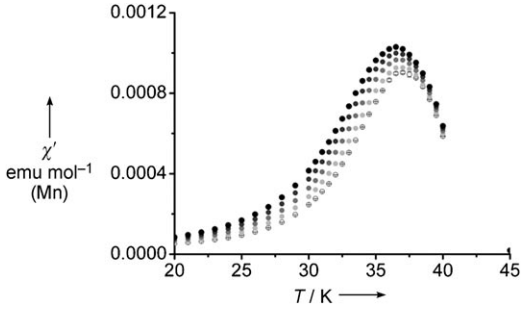

Figure 5. Real part of the AC susceptibility of the Mn_3O_4 nanoparticle array measured at frequencies ranging from 1 Hz (closed circles) through 6, 40, and 250 to 1588 Hz (open circles).

The relation between T_B and ν for a superparamagnet is expected to exhibit an Arrhenius form [Eq. (1)]:[13]

$$\nu = \nu_o \exp(-E_a/R\,T_B) \quad (1)$$

where ν_o is a characteristic relaxation time, commonly 10^{-9}–10^{-13} s for isolated superparamagnetic particles, and E_a is usually considered to relate to an activation barrier for magnetization reversal. A least-squares fit to this relation is displayed in Figure 6, which shows the relation between $\ln \nu$

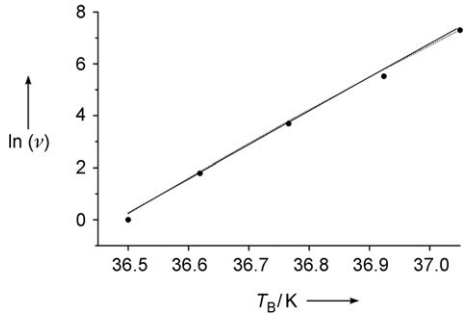

Figure 6. Relation between the frequency of the measurement (ν, in Hertz), and the blocking temperature (T_B) with a least-squares fit to an Arrhenius expression (——) and the Vogel–Fulcher law (•••••).

and T_B, where T_B corresponds to the maximum in χ'. Optimized parameters are $\nu_o = 10^{178(4)}$ s and $E_a/R = 17620$-(394) K. Both these are physically unrealistic for a superparamagnet; rather, they are compatible with those found in spin-glass systems and interacting magnetic nanoparticles.[14,15]

The frequency dependence of T_B for such systems is most commonly analyzed using the phenomenological Vogel–Fulcher expression, which is taken from the glass literature (Eq. (2)):

$$\nu = \nu_o \exp(-E_a/R(T_B - T_0)) \quad (2)$$

The parameter T_0 is sometimes taken to represent the inter-particle coupling strength, and is smaller—usually considerable smaller—than T_B.[15] Least-squares fitting of this expression for the data taken on the array (Figure 6) revealed a very strong correlation between the variables ν_o, E_a, and T_0; the following values were found for a free fit of all variables: $\nu_o = 10^{35(1)}$ s, $E_a/R = 625(13)$ K, and $T_0 = 29(7)$ K. Physically reasonable values of ν_o and E_a/R are only found when T_0 approaches T_B, indicating that the magnetic forces acting on the particles are comparable in strength to those within the particles. It is unlikely that such forces could arise from coupling between the particles, given the surface coating of amines, but it could indicate coupling between a core of Mn_3O_4 and a shell of a chemically modified form of the core material. The PXRD, HRTEM, and SAED results revealed no evidence for any other crystalline material except Mn_3O_4. Confirmation that the magnetic interactions occur between core and shell rather than between particles was obtained by dispersing the particles in hexane and measuring the magnet-

ization, which was identical to that observed for the nanoparticle array.

To investigate whether a shell of different material is present, X-ray photoelectron spectroscopy (XPS) was carried out. Bulk Mn_3O_4 and β-MnO_2 were also measured for comparison. The Mn $2p^{3/2}$, Mn $2p^{1/2}$, and O 1s binding energies for the nanoparticles, Mn_3O_4, and β-MnO_2 are shown in Table 1. It is evident that the manganese atoms at the surface

Table 1: XPS binding energy for bulk Mn_3O_4, bulk β-MnO_2, and a Mn_3O_4 nanoparticle array.

Sample	Peak position [eV]		
	Mn $2p^{3/2}$	Mn $2p^{1/2}$	O 1s
bulk Mn_3O_4	641.2	652.7	529.6
bulk β-MnO_2	642.5	653.9	529.5
Mn_3O_4 nanoparticle array	642.2	653.7	530.1

of the Mn_3O_4 nanoparticle array have binding energies close to those of bulk MnO_2 rather than bulk Mn_3O_4. A peak associated with the N 1s binding energy, owing to the RNH_2 molecules on the surface, was also observed. We propose that the particles are composed of a core of Mn_3O_4 encapsulated in a shell of MnO_2, to which the RNH_2 molecules are attached. Given that the MnO_2 shell is not observed by PXRD, SAED, or HRTEM, we conclude that the MnO_2 layer must be thin (less than 1 nm) and is probably disordered. As a result, the shell is likely to have significant degrees of spin disorder and likely to couple to the core phase through significant superexchange interactions. An increasing number of magnetic core–shell systems, or granular materials, with similar types of components are being characterized and are generally found to have some degree of spin-glass character, as discussed herein.[16]

In conclusion, an ordered (predominantly cubic) three-dimensional array of monodispersed Mn_3O_4 nanoparticles (diameter ca. 8 nm) with a core–shell structure has been prepared for the first time by a one-step thermal decomposition of [Mn(acac)$_2$] in oleylamine. PXRD, HRTEM, and XPS results confirmed that these particles have a highly crystalline Mn_3O_4 core encapsulated within a thin shell of MnO_2. FTIR data indicate that the shell is capped by oleylamine. The self-assembled three-dimensional arrays exhibit interesting behavior similar to a spin-glass material rather than the superparamagnetic behavior anticipated for isolated nanoparticles. This difference may be due to the strong interaction between core (Mn_3O_4) and shell (MnO_2).

Experimental Section

The procedure for synthesizing Mn_3O_4 nanoparticles was developed by modifying a procedure reported previously.[3] In a typical synthesis, a mixture of [Mn(acac)$_2$] (1 g, 3.74 mmol; Aldrich) and oleylamine (20-mL; ≥ 70 %, Fluka), was placed in a three-neck 250 mL flask and heated rapidly (15 min to 210 °C) with continuous stirring under air. The color of the mixture turned from yellow to dark brown. The temperature was maintained at 210 °C for 5 h and the mixture then cooled to room temperature. After addition of 30 mL of ethanol, the product was centrifuged and the liquid separated off. This process was repeated twice to remove remaining unreacted surfactant. The final product was again dispersed in ethanol (10 mL) in an ultrasonic bath for 3 minutes, followed by drying at 50 °C for 2 days.

The isolated particles and the arrays were examined by TEM. For the particles, a small amount of powder was dispersed in hexane, and the mixture was dropped onto a carbon-coated TEM grid with subsequent evaporation of the hexane at room temperature. For the arrays, a small amount of powder was lightly ground with some ethanol, and a drop of the mixture was placed on the TEM grid.

TEM was carried out using a JEOL JEM-2011 instrument. Wide-angle powder X-ray diffraction data were collected on a Stoe STADI/P powder diffractometer operating in transmission mode with a small-angle position-sensitive detector. Incident radiation was generated using an $Fe_{K\alpha 1}$ source ($\lambda = 1.936$ Å). The XPS data were collected using a VG ESCALAB II spectrometer with an operating pressure of 1×10^{-9} mbar and non-monochromated $Al_{K\alpha}$ radiation (1486.6 eV). The sample area was of 3-mm diameter. Peaks were recorded with a constant step energy of 0.05 eV and a pass energy of 20 eV. The binding energy scale was calibrated with the C1s line of carbon at 284.6 eV. DC magnetization data were collected for Mn_3O_4 nanoparticles in the form of a dry powder. The sample was loaded into gelatine capsules and measured on a Quantum Design $MPMS_2$ SQUID magnetometer from 1.8 K to 340 K, in fields of 0.01 T after cooling first in zero field (zfc), and then in the 0.01-T field (fc). The AC susceptibility was also measured using frequencies from 1 to 1488 Hz, a drive amplitude of 0.1 mT, and no DC field.

Received: January 8, 2007
Revised: February 12, 2007
Published online: April 19, 2007

Keywords: magnetic properties · nanoparticles · self-assembly · spin glass · spinel phases

[1] a) A. P. Alivisatos, *Science* **1996**, *271*, 933; b) S. Polarz, F. Neues, M. W. E. van den Berg, W. Grunert, L. Khodeir, *J. Am. Chem. Soc.* **2005**, *127*, 12028; c) S. Carrettin, P. Concepcion, A. Corma, J. M. L. Nieto, V. F. Puntes, *Angew. Chem.* **2004**, *116*, 2592; *Angew. Chem. Int. Ed.* **2004**, *43*, 2538; d) M. H. Cao, T. F. Liu, S. Gao, G. B. Sun, X. L. Wu, C. W. Hu, Z. L. Wang, *Angew. Chem.* **2005**, *117*, 4269; *Angew. Chem. Int. Ed.* **2005**, *44*, 4197.

[2] a) D. Larcher, G. Sudant, J. B. Leriche, Y. Chabre, J. M. Tarascon, *J. Electrochem. Soc.* **2003**, *150*, A133; b) S. Grugeon, S. Laruelle, R. Herrera-Urbina, L. Dupont, P. Poizot, J. M. Tarascon, *J. Electrochem. Soc.* **2001**, *148*, A285.

[3] W. S. Seo, H. H. Jo, K. Lee, B. Kim, S. J. Oh, J. T. Park, *Angew. Chem.* **2004**, *116*, 1135; *Angew. Chem. Int. Ed.* **2004**, *43*, 1115.

[4] a) V. F. Puntes, K. M. Krishnan, A. P. Alivisatos, *Science* **2001**, *291*, 2115; b) H. M. Chen, R. S. Liu, H. L. Li, H. C. Zeng, *Angew. Chem.* **2006**, *118*, 2779; *Angew. Chem. Int. Ed.* **2006**, *45*, 2713; c) X. Wang, J. Zhuang, Q. Peng, Y. D. Li, *Nature* **2005**, *437*, 121; d) M. Yin, C. K. Wu, Y. B. Lou, C. Burda, J. T. Koberstein, Y. M. Zhu, S. O'Brien, *J. Am. Chem. Soc.* **2005**, *127*, 9506; e) S. H. Sun, H. Zeng, D. B. Robinson, S. Raoux, P. M. Rice, S. X. Wang, G. X. Li, *J. Am. Chem. Soc.* **2004**, *126*, 273; f) S. O'Brien, L. Brus, C. B. Murray, *J. Am. Chem. Soc.* **2001**, *123*, 12085.

[5] T. Hyeon, S. S. Lee, J. Park, Y. Chung, H. Bin Na, *J. Am. Chem. Soc.* **2001**, *123*, 12798.

[6] a) W. S. Seo, J. H. Shim, S. J. Oh, E. K. Lee, N. H. Hur, J. T. Park, *J. Am. Chem. Soc.* **2005**, *127*, 6188; b) C. Petit, A. Taleb, M. P. Pileni, *J. Phys. Chem. B* **1999**, *103*, 1805; c) M. P. Pileni, *Appl. Surf. Sci.* **2001**, *171*, 1; d) R. Pozas, A. Mihi, M. Ocana, H. Miguez, *Adv. Mater.* **2006**, *18*, 1183.

[7] a) M. Yin, S. O'Brien, *J. Am. Chem. Soc.* **2003**, *125*, 10180; b) O. Giraldo, S. L. Brock, W. S. Willis, M. Marquez, S. L. Suib, S.

Ching, *J. Am. Chem. Soc.* **2000**, *122*, 9330; c) M. M. Thackeray, *Prog. Solid. State Chem.* **1997**, *25*, 1.
[8] M. F. Casula, Y. W. Jun, D. J. Zaziski, E. M. Chan, A. Corrias, A. P. Alivisatos, *J. Am. Chem. Soc.* **2006**, *128*, 1675.
[9] a) M. Rajamathi, M. Ghosh, R. Seshadri, *Chem. Commun.* **2002**, 1152; b) M. J. Hostetler, J. J. Stokes, R. W. Murray, *Langmuir* **1996**, *12*, 3604.
[10] S. Mandal, S. R. Sainkar, M. Sastry, *Nanotechnology* **2001**, *12*, 358.
[11] a) K. Dwight, N. Menyuk, *Phys. Rev. B* **1960**, *119*, 1470; b) G. B. Jensen, O. V. Nielsen, *J. Phys. C* **1974**, *7*, 409; c) G. Srinivasan, M. S. Seehra, *Phys. Rev. B* **1983**, *28*, 1; d) I. S. Jacobs, *J. Phys. Chem. Solids* **1959**, *11*, 1.
[12] Y. Q. Chang, X. Y. Xu, X. H. Luo, C. P. Chen, D. P. Yu, *J. Cryst. Growth* **2004**, *264*, 232.
[13] a) L. Neel, *Ann. Geophys.* **1949**, *5*, 99; b) W. F. Brown, *Phys. Rev.* **1963**, *130*, 1677.
[14] a) A. Mydosh, *Spin Glasses: an Experimental Introduction*, Taylor and Francis, London **1993**; b) J. L. Dormann, L. Bessais, D. Fiorani, *J. Phys. C* **1988**, *21*, 2015; c) J. L. Dormann, F. D'Orazio, F. Lucari, E. Tronc, P. Prene, J. P. Jolivet, D. Fiorani, R. Cherkaoui, M. Nogues, *Phys. Rev. B* **1996**, *53*, 14291.
[15] S. Shtrikman, E. P. Wohlfarth, *Phys. Lett. A* **1981**, *85*, 467.
[16] a) S. Gangopadhyay, G. C. Hadjipanayis, B. Dale, C. M. Sorensen, K. J. Klabunde, V. Papaefthymiou, A. Kostikas, *Phys. Rev. B* **1992**, *45*, 9778; b) A. Hernando, *J. Phys. Condens. Matter* **1999**, *11*, 9455; c) E. Tronc, A. Ezzir, R. Cherkaoui, C. Chaneac, M. Nogues, H. Kachkachi, D. Fiorani, A. M. Testa, J. M. Greneche, J. P. Jolivet, *J. Magn. Magn. Mater.* **2000**, *221*, 63; d) M. Muroi, P. G. McCormick, J. Amighian, *Phys. Rev. B* **2001**, *63*, 184414; e) L. Del Bianco, D. Fiorani, A. M. Testa, E. Bonetti, L. Savini, S. Signoreti, *Phys. Rev. B* **2002**, *66*, 174418; f) Q. A. Pankhurst, A. Y. Martinez, L. F. Barquin, *Phys. Rev. B* **2004**, 69, 212401; g) N. S. Gajbhiye, S. Bhattacharyya, *Nanotechnology* **2005**, *16*, 2012.

